\



Probing the magnetization switching with in-plane magnetic anisotropy through field-modified magnetoresistance measurement

Runrun Hao(郝润润), Kun Zhang(张昆), Yinggang Li(李迎港), Qiang Cao(曹强), Xueying Zhang(张学莹), Dapeng Zhu(朱大鹏), and Weisheng Zhao(赵巍胜)

Citation: Chin. Phys. B, 2022, 31 (**1**): 017502. DOI: 10.1088/1674-1056/ac21bb
Journal homepage: http://cpb.iphy.ac.cn; http://iopscience.iop.org/cpb

What follows is a list of articles you may be interested in

Observation of magnetoresistance in CrI_3/graphene van der Waals heterostructures

Yu-Ting Niu(牛宇婷), Xiao Lu(鲁晓), Zhong-Tai Shi(石钟太), and Bo Peng(彭波)
Chin. Phys. B, 2021, 30 (**11**): 117506. DOI: 10.1088/1674-1056/ac1e1d

Vertical WS_2 spin valve with Ohmic property based on Fe_3GeTe_2 electrodes

Ce Hu(胡策), Faguang Yan(闫法光), Yucai Li(李予才), and Kaiyou Wang(王开友)
Chin. Phys. B, 2021, 30 (**9**): 097505. DOI: 10.1088/1674-1056/ac078b

Current-dependent positive magnetoresistance in$La_{0.8}Ba_{0.2}MnO_3$ ultrathin films

Guankai Lin(林冠凯), Haoru Wang(王昊儒), Xuhui Cai(蔡旭晖), Wei Tong(童伟), and Hong Zhu(朱弘)
Chin. Phys. B, 2021, 30 (**9**): 097502. DOI: 10.1088/1674-1056/ac012d

Experiments and SPICE simulations of double MgO-based perpendicular magnetic tunnel junction

Qiuyang Li(李求洋), Penghe Zhang(张蓬鹤), Haotian Li(李浩天), Lina Chen(陈丽娜), Kaiyuan Zhou(周恺元), Chunjie Yan(晏春杰), Liyuan Li(李丽媛), Yongbing Xu(徐永兵), Weixin Zhang(张卫欣), Bo Liu(刘波), Hao Meng(孟浩), Ronghua Liu(刘荣华), and Youwei Du(都有为)
Chin. Phys. B, 2021, 30 (**4**): 047504. DOI: 10.1088/1674-1056/abdea2

Field-induced N\'eel vector bi-reorientation of a ferrimagnetic insulator in the vicinity of compensation temperature

Peng Wang(王鹏), Hui Zhao(赵辉), Zhongzhi Luan(栾仲智), Siyu Xia(夏思宇), Tao Feng(丰韬), and Lifan Zhou(周礼繁)
Chin. Phys. B, 2021, 30 (**2**): 027501. DOI: 10.1088/1674-1056/abbbef

---

RAPID COMMUNICATION

Probing the magnetization switching with in-plane magnetic anisotropy through field-modified magnetoresistance measurement

Runrun Hao(郝润润)[1,2,†], Kun Zhang(张昆)[1,2,†], Yinggang Li(李迎港)[1,2], Qiang Cao(曹强)[3], Xueying Zhang(张学莹)[1,2,4,‡], Dapeng Zhu(朱大鹏)[1,2,§], and Weisheng Zhao(赵巍胜)[1,2]

[1] *Fert Beijing Institute, MIIT Key Laboratory of Spintronics, School of Integrated Circuit Science and Engineering, Beihang University, Beijing* 100191, *China*

[2] *Beihang-Goertek Joint Microelectronics Institute, Qingdao Research Institute, Beihang University, Qingdao* 266000, *China*

[3] *Spintronics Institute, University of Jinan, Jinan* 250022, *China*

[4] *Truth Instruments Co. Ltd., Qingdao* 266000, *China*

(Received 11 July 2021; revised manuscript received 23 August 2021; accepted manuscript online 27 August 2021)

Effective probing current-induced magnetization switching is highly required in the study of emerging spin–orbit torque (SOT) effect. However, the measurement of in-plane magnetization switching typically relies on the giant/tunneling magnetoresistance measurement in a spin valve structure calling for complicated fabrication process, or the non-electric approach of Kerr imaging technique. Here, we present a reliable and convenient method to electrically probe the SOT-induced in-plane magnetization switching in a simple Hall bar device through analyzing the MR signal modified by a magnetic field. In this case, the symmetry of MR is broken, resulting in a resistance difference for opposite magnetization orientations. Moreover, the feasibility of our method is widely evidenced in heavy metal/ferromagnet (Pt/$Ni_{20}Fe_{80}$ and W/$Co_{20}Fe_{60}B_{20}$) and the topological insulator/ferromagnet (Bi_2Se_3/$Ni_{20}Fe_{80}$). Our work simplifies the characterization process of the in-plane magnetization switching, which can promote the development of SOT-based devices.

Keywords: magnetoresistance, in-plane magnetization switching, electrical detection

PACS: 75.47.–m, 85.75.–d, 71.70.Ej **DOI:** 10.1088/1674-1056/ac21bb

1. Introduction

In recent years, intensive attention has been paid to the 3-terminal spintronic device with information written by the spin–orbit torque (SOT) effect, which allows a high writing speed without incubation delay and has an enhanced endurance benefiting from the separated read/write routes.[1–3] One typical SOT device employs a heavy metal/ferromagnet (HM/FM) heterostructure as the basic function structure for the information writing, where the spin current induced by an in-plane charge current via the spin–orbit interactions (SOI) of the HM layer will exert spin torques on the magnetization and drive magnetization switching of the adjacent FM layer.[4–9] In terms of the easy-axis direction of the FM layer, the SOT devices mainly take one of the two configuration types: the easy-axis perpendicular to the film plane,[6,10,11] or, the easy-axis lying in the film plane and orthogonal to the charge current.[4] A lot of experimental techniques, such as spin torque ferromagnetic resonance (ST-FMR) or harmonic Hall experiments, have been developed to characterize the SOT efficiency in these devices.[12–17]

On the other hand, the SOT-induced magnetization switching is technologically more relevant to the device applications, thus the efficient probing of the SOT-induced magnetization switching is also of great significance. For the FM with perpendicular magnetic anisotropy (PMA), the magnetization switching can be easily probed by measuring the anomalous Hall effect (AHE).[5,6,18] However, for the FM with in-plane magnetic anisotropy (IMA), the Hall voltage or magnetoresistance (MR) measurements can not evidence the magnetization switching due to their equal resistance values for opposite magnetization orientations. The SOT-induced magnetization switching in the HM/FM heterostructure with IMA are typically probed by giant magnetoresistance (GMR)/tunneling magnetoresistance (TMR) in a spin valve structure.[19,20] The complicated device fabrication process hinders this technique being developed into a widely used approach to detect SOT switching. The magneto-optic Kerr effect (MOKE) imaging technique can also probe in-plane magnetization switching,[21,22] but suffers drawbacks of being applicable only to the devices with thin capping and having bad capability with low temperature and strong magnetic field. A convenient access to probe the SOT-induced magnetization switching of an FM with IMA is still highly desired.

For FM with IMA, there is no difference in resistance for the magnetization oriented to opposite directions, as shown in Fig. 1(a). If a magnetic field (H) is applied to break the

†These authors contributed equally to this work.

‡Corresponding author. E-mail: xueying.zhang@buaa.edu.cn

§Corresponding author. E-mail: zhudp@buaa.edu.cn

© 2022 Chinese Physical Society and IOP Publishing Ltd

symmetry of the MR signal, the difference in resistance arises, i.e., high-resistance-state (high-R state) or low-resistance-state (low-R state) occurs for the magnetization antiparallel or parallel to H, respectively,[23] as shown in Fig. 1(b). Inspired by this principle, we provide a convenient electrical strategy to probe the SOT-induced magnetization switching with IMA. For the material system with strong field-like SOT,[24] the resulting effective field when current flowing through HM would break the symmetry and result in resistance difference for opposite magnetization orientations, thus allowing the electrically probing of the magnetic state. Furthermore, an appropriate external magnetic field can replace the field-like effective field to modify the MR signal, which is suitable for more extensive material systems, not only the one with strong field-like torque. We observe clear SOT switching loops and demonstrate the feasibility of these methods in probing the SOT driven magnetization switching in various systems of Pt/NiFe, W/CoFeB and Bi_2Se_3/NiFe Hall bars with IMA. The method with MR modified by an external magnetic field enables a small reading current, which can avoid thermal noise and possible even damage on microstructure device due to the persistent Joule heating. This work provides an effective and reliable method to electrically characterize the in-plane magnetization switching in a simple Hall bar, which can facilitate the study of SOT-related effect.

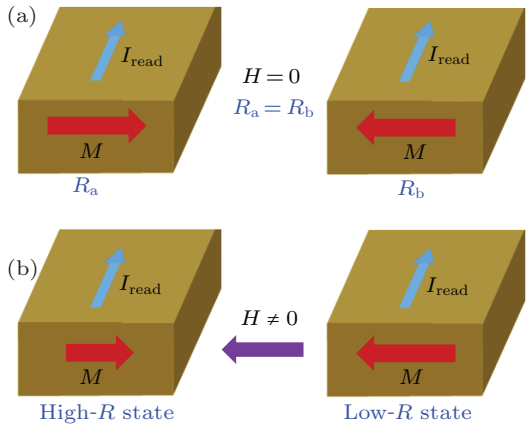


Fig. 1. Schematic diagrams of resistance states of FM layer for magnetization oriented to opposite directions (a) without or (b) with a modifying field.

2. Experimental details

The Pt(6)/$Ni_{20}Fe_{80}$(8) and W(5)/$Co_{20}Fe_{60}B_{20}$(1.9) bilayers (the thicknesses in the parentheses are in nanometers) are prepared on thermally oxidized Si substrates with a magnetron sputtering system at room temperature, and the base pressure is better than 5×10^{-6} Pa. As for the Bi_2Se_3(8)/$Ni_{80}Fe_{20}$(3.5) bilayers, the high-quality Bi_2Se_3 films are grown on Al_2O_3 (0001) substrates in a molecular beam epitaxy (MBE) system with a base pressure better than 2×10^{-7} Pa, by using the two-step deposition procedure, and then the $Ni_{80}Fe_{20}$ film is subsequently sputtered on the Bi_2Se_3 film at room temperature. For MR and SOT switching measurements, the as-deposited films are patterned into Hall bars with channel sizes of 10 μm×80 μm through photolithography and Ar ion milling processes. All measurements are performed at room temperature using a home-made magneto-electrical transport measurement system. A current source of Keithley 6221 and a nano-voltmeter of Keithley 2182 are used to supply dc read currents ($I_{\rm read}$) and detect dc voltages (V), respectively. The longitudinal resistance $R_{xx} = V/I_{\rm read}$. The pulse currents ($I_{\rm pulse}$) with pulse duration of 10 μs for switching the magnetization are supplied by Keithley 4200.

3. Results and discussion

The MR measurement with a four-point probe method for Pt/$Ni_{20}Fe_{80}$ is schematically shown in Fig. 2(a). We inject the charge current (including $I_{\rm read}$ and $I_{\rm pulse}$) and measure the voltage along x axis with external magnetic fields $H_{\rm ext}$ sweeping along y axis. As shown in Fig. 2(b), the magnetization of the Pt/$Ni_{80}Fe_{20}$ is characterized by MR measurement with $I_{\rm read} = -0.1$ mA, and the coercive field of about 5.2 Oe is obtained. The normalized MR loops with $I_{\rm read} = \pm4$ mA are shown in Fig. 2(c). For $I_{\rm read} = \pm4$ mA, obvious horizontal shifts of the MR peaks are observed, indicating the existence of a current-induced effective field $H_{\rm CEF}$.[25–27] The critical magnetization switching fields $H_{\rm SW}$ for different $I_{\rm read}$ are shown in Fig. 2(d), where $H_{\rm SW}^{+}$ or $H_{\rm SW}^{-}$ are the critical magnetization switching fields for external fields sweeping from $-y$ to $+y$ or from $+y$ to $-y$, respectively. We find that $H_{\rm SW}^{+}$ and $H_{\rm SW}^{-}$ are both proportional to the value of $I_{\rm read}$, and $H_{\rm CEF} = (H_{\rm SW}^{+} + H_{\rm SW}^{-})/2$ is reversed when the sign of $I_{\rm read}$ is changed. For $|I_{\rm read}| = 4$ mA, the Oster field $H_{\rm Oe}$ induced acting on the $Ni_{80}Fe_{20}$ layer is calculated to be much smaller than $H_{\rm CEF} \approx 2.5$ Oe. Hence, the horizontal shift in the MR loop mainly origins from the field-like effective field induced by the SOT effect.

The magnetization switching measurements of the Pt/$Ni_{80}Fe_{20}$ Hall bar with the modification of $H_{\rm CEF}$ are performed. Figures 3(a) and 3(b) illustrate the process diagrams of these measurements. The pulse current $I_{\rm pulse}$ sweeps from negative to positive values and back to negative values. After each of pulse currents, read currents of $I_{\rm read} = \pm3$ mA are injected to modify MR signals and detect the corresponding voltages. The longitudinal resistance R_{xx} versus pulse current $I_{\rm pulse}$ is shown in Figs. 3(c) and 3(d). It is found that R_{xx} switches to the high-R state or low-R state at critical switching pulse currents of $I_{\rm pulse} \approx \mp5.5$ mA, respectively. The measured critical switching current is well reproducible after several switching cycles. And the polarities of the pulse current-induced switch-

ing loops are opposite for $I_{\rm read} = \pm 3$ mA. The origin of variation in R_{xx} when the magnetization switching takes place is schematically shown in Figs. 3(e) and 3(f). Under the modification of large $H_{\rm CEF}$, the states with magnetization along $\pm y$ directions have different R_{xx} values. When the damping-like torque induced by the $I_{\rm pulse}$ is large enough to overcome the intrinsic damping and switches the magnetization, a variation in R_{xx} occurs with the modification of $H_{\rm CEF}$.

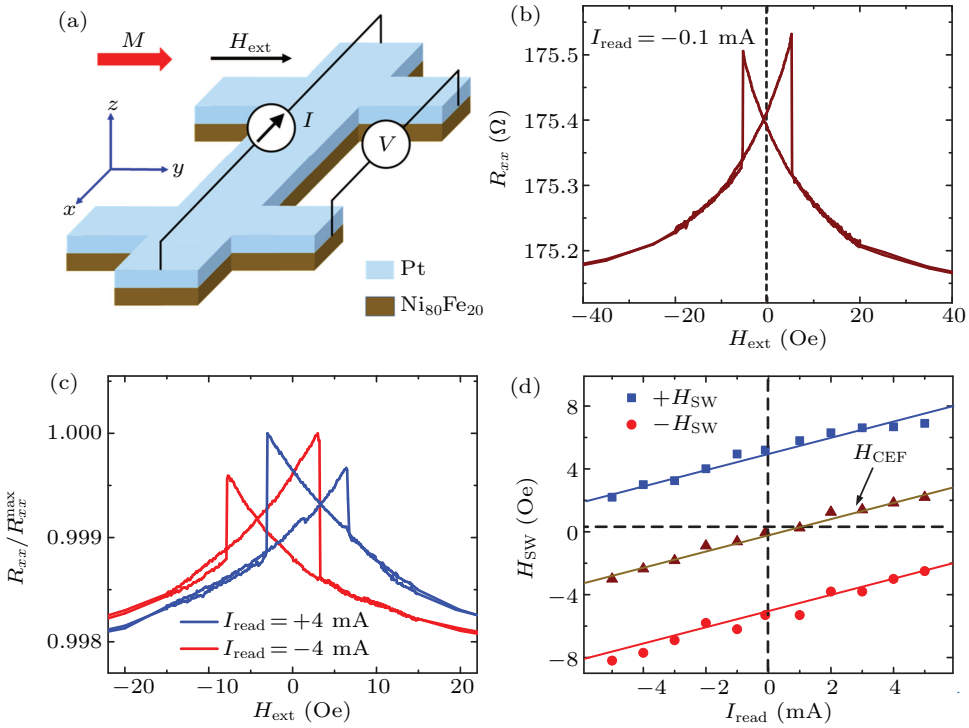


Fig. 2. (a) Schematic illustration of the Pt/$Ni_{80}Fe_{20}$ Hall bar device with channel size of 10 μm×80 μm and MR measurement. The positive direction of current is defined along the $-x$ direction, and the positive direction of the external magnetic field is defined along the $+y$ direction. (b) The MR loop for Pt/$Ni_{80}Fe_{20}$ Hall bar with $I_{\rm read} = -0.1$ mA. (c) The shifted MR loops for Pt/$Ni_{80}Fe_{20}$ Hall bar with $I_{\rm read} = \pm 4$ mA. (d) The critical switching field $H_{\rm SW}$ versus read current $I_{\rm read}$ for Pt/$Ni_{80}Fe_{20}$ Hall bar. The $H_{\rm CEF} = (H_{\rm SW}^{+} + H_{\rm SW}^{-})/2$, where $H_{\rm SW}^{+}$ or $H_{\rm SW}^{-}$ are the critical switching fields for external field $H_{\rm ext}$ sweeping from $-y$ to $+y$ or from $+y$ to $-y$, respectively.

As can be seen from the above results, the MR modified by $H_{\rm CEF}$ can be used to probe SOT-induced switching in the heterostructure with IMA. Note that the requirement for a sizeable $H_{\rm CEF}$ may be an important limitation for this method. For the stacks with small $H_{\rm CEF}$,[12,28] there is no significant difference in R_{xx} for opposite magnetization orientations. This limitation can be eliminated by introducing an appropriate external assisting field $H_{\rm assist}$. Next, we demonstrate the probing of SOT-induced magnetization switching of the Pt/$Ni_{80}Fe_{20}$ heterostructure under the modification of $H_{\rm assist}$. The process diagrams of the switching measurements with the assisting fields of $H_{\rm assist} = \mp 1.2$ Oe are illustrated in Figs. 4(a) and 4(b), respectively. The pulse currents $I_{\rm pulse}$ sweep from negative to positive values and back to negative values. After each of $I_{\rm pluse}$, a small read current of $I_{\rm read} = +0.1$ mA and an $H_{\rm assist}$ are applied simultaneously to detect the corresponding resistance. As shown in Fig. 4(c), with $H_{\rm assist} = -1.2$ Oe, the R_{xx} switches to low-R state at around $I_{\rm pluse} = +5.5$ mA, and it switches back to high-R state at around $I_{\rm pluse} = -5.5$ mA. And the polarities of switching loops change with the sign reversal of $H_{\rm assist}$, as shown in Fig. 4(d). The origin of difference in R_{xx} between the opposite magnetization orientations is schematically shown in Figs. 4(e) and 4(f). For $|I_{\rm read}| = 0.1$ mA, the $H_{\rm CEF}$ is negligibly small as shown in Fig. 2(b). The $H_{\rm assist}$ plays the similar role in modifying R_{xx} to that of $H_{\rm CEF}$, where the R_{xx} value depends on the relative orientation between the magnetization and $H_{\rm assist}$. Comparing the above two methods, the former one that modified by $H_{\rm CEF}$ requires a relatively simple equipment, but is infeasible for the systems with small field-like torque. In addition, the required giant reading current and subsequent persistent Joule heating may introduce remarkable thermal noise and even damage the microstructure device. In contrast, the latter one that modified by $H_{\rm assist}$ allows a small read current and caters for more extensive material systems, which is a universal, reliable and effective method.

Based on the measured results, we can estimate the SOT efficiency of the Pt/$Ni_{80}Fe_{20}$ heterostructure. The field-like SOT efficiency ($\xi_{\rm FL}$) can be written as[29,30]

$$\xi_{\rm FL} = \frac{2e\mu_0}{\hbar} M_{\rm S} t_{\rm NiFe} \left(\frac{H_{\rm FL}}{J_{\rm Pt}} \right), \tag{1}$$

and the damping-like SOT efficiency ($\xi_{\rm DL}$) can be written as[31–33]

$$\xi_{\rm DL} = \frac{2e\mu_0}{\hbar} M_{\rm S} t_{\rm NiFe} \alpha_0 \left(\frac{H_{\rm c} + M_{\rm k}/2}{J_{\rm c0}} \right), \tag{2}$$

where M_S, t_{NiFe}, $\mu_0 M_k$, and J_{Pt} are the saturation magnetization, thickness of the $Ni_{80}Fe_{20}$ layer, demagnetization field, and current density flowing in the Pt layer, respectively. The $H_{FL} = H_{CEF} - H_{Oe}$ is the field-like effective field acting on the $Ni_{80}Fe_{20}$ layer, which is proportional to J_{Pt}. With pulse current duration ranging from 5 μs to 0.5 s, the critical switching current almost keeps a constant. Therefore, the zero-thermal-fluctuation critical switching current density J_{c0} should be approximately equal to the critical switching current density J_c for our sample.[33] The damping constant $\alpha_0 \approx 0.015$ and $\mu_0 M_k \approx 0.92$ T are determined by ferromagnetic resonance (FMR) measurements. With Eqs. (1) and (2), the field-like SOT efficiency $\xi_{FL} = 0.01$ and the damping-like SOT efficiency $\xi_{DL} = 0.23$ are obtained for the Pt/$Ni_{80}Fe_{20}$ heterostructure, respectively. The calculated ξ_{FL} and ξ_{DL} are comparable to the values reported in previous works.[25,30,34,35]

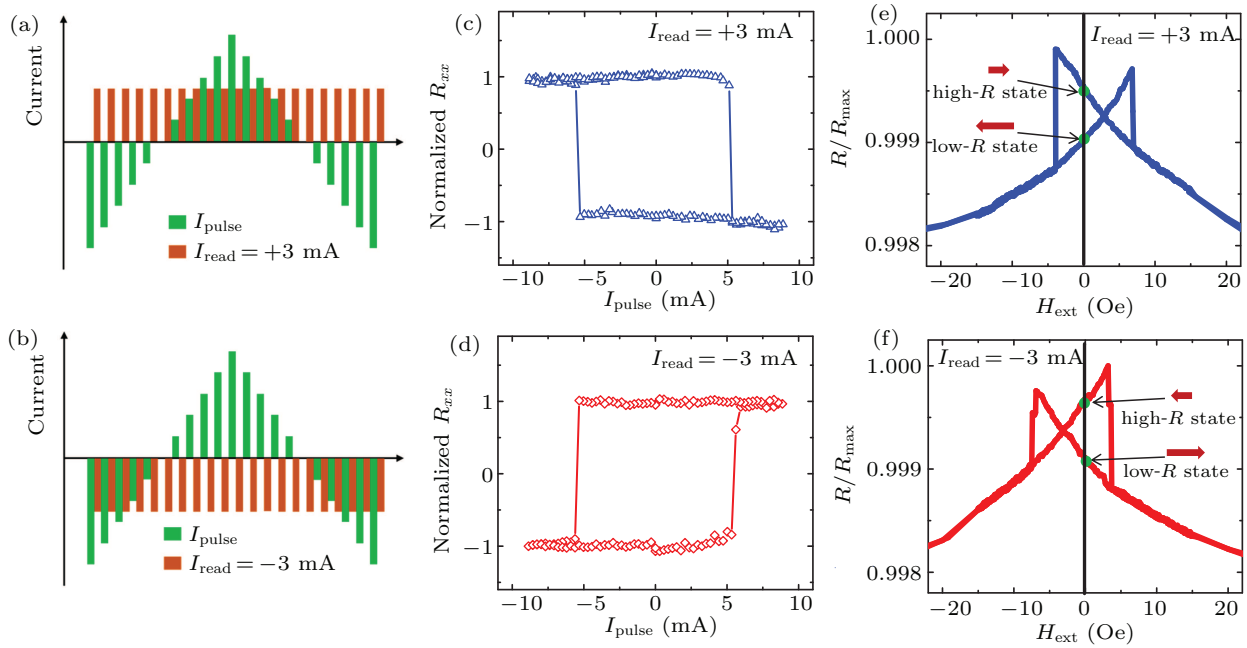


Fig. 3. The magnetization switching measurement with MR modified by the current-induced effective field H_{CEF} for Pt/$Ni_{80}Fe_{20}$ Hall bar. (a), (b) The measurement processes for the switching experiments with read currents of $I_{read} = \pm 3$ mA, respectively. (c), (d) The variation in resistance versus pulse current with $I_{read} = \pm 3$ mA, respectively. (e), (f) The difference in resistance for opposite magnetization orientations with positive and negative read currents, respectively.

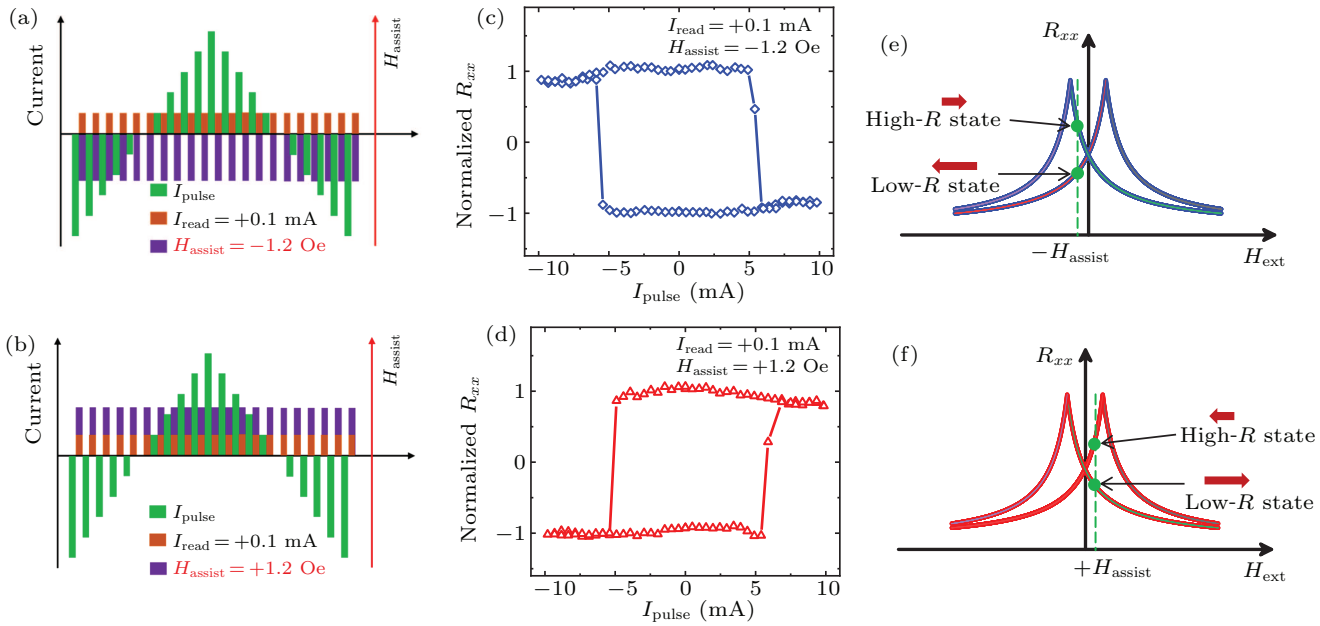


Fig. 4. The magnetization switching measurement with MR modified by the external magnetic field for Pt/$Ni_{80}Fe_{20}$ Hall bar. (a), (b) The measurement processes for switching experiments with read current of $I_{read} = +0.1$ mA. During the measurements of R_{xx}, the assisting fields of $H_{assist} = \mp 1.2$ Oe are applied, respectively. (c), (d) The variation in resistance versus pulse current with assisted fields of $H_{assist} = \mp 1.2$ Oe, respectively. (e), (f) Schematic diagrams of difference in resistance for opposite magnetization orientations under the modification of negative and positive assisting fields, respectively.

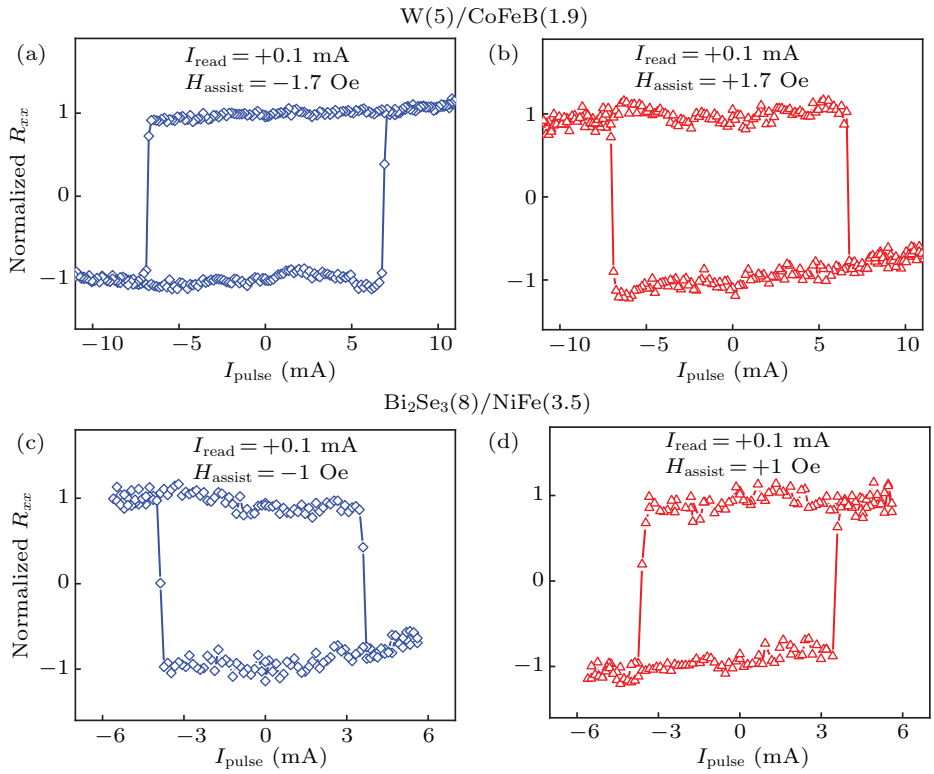


Fig. 5. (a), (b) The variation in resistance versus pulse current for W/$Co_{20}Fe_{60}B_{20}$ Hall bar with assisted fields of $H_{assist} = \mp 1.7$ Oe, respectively. (c), (d) The variation in resistance versus pulse current for Bi_2Se_3/$Ni_{80}Fe_{20}$ Hall bar with assisted fields of $H_{assist} = \mp 1$ Oe, respectively.

To further verify the feasibility and application range of our method, the magnetization switching measurements with R_{xx} modified by the H_{assist} are also performed in different material systems. The R_{xx} versus the magnetic field of a W/$Co_{20}Fe_{60}B_{20}$ Hall bar with $H_{assist} = \mp 1.7$ Oe is shown in Figs. 5(a) and 5(b), respectively. The switching of R_{xx} between high-R state and low-R state takes place at $I_{pluse} = \pm 6.8$ mA. The polarities of the switching loops are reversed when the HM layer is changed from Pt to W for H_{assist} with the same sign since Pt and W possess opposite signs of the spin Hall angle. It is worth noting that the measured signal of W/$Co_{20}Fe_{60}B_{20}$ in our experiments is comparable to that of Pt/$Ni_{80}Fe_{20}$.[36] Meanwhile, the anisotropy MR (AMR) ratio of $Co_{20}Fe_{60}B_{20}$ single layer is about one order smaller than that of $Ni_{80}Fe_{20}$.[37,38] These results mean that the spin MR (SMR), proportional to the square of the HM layer's spin Hall angle,[23] plays a dominant role in the electrical measurement of magnetization switching in the W/$Co_{20}Fe_{60}B_{20}$ sample. Therefore, our method is suitable for various FM materials, even those with weak common AMR. Furthermore, our method is extended to the emerging topological insulator of Bi_2Se_3 with large charge-to-spin conversion efficiency and the magnetization switching measurements of Bi_2Se_3/$Ni_{80}Fe_{20}$ Hall bar are performed.[39] The clear switching of R_{xx} at $|I_{pluse}| = 3.4$ mA with $H_{assist} = \mp 1$ Oe is observed in Figs. 5(c) and 5(d), respectively. With Eq. (2), the damping-like SOT efficiency ξ_{DL} of Bi_2Se_3/$Ni_{80}Fe_{20}$ is estimated to be 0.91 which is roughly consistent with the previous report.[22] The above results strongly demonstrate that our method can be used to effectively determine the SOT efficiency for various material systems with IMA.

4. Conclusion

In summary, with the modification of a current-induced effective field or an external assisting field, the switching symmetry of MR is broken and the difference in resistance is induced for opposite magnetization orientations, allowing the electrical probing of in-plane magnetization switching in a simple Hall bar device. The method by utilizing an assisting field can be employed for various material systems, even for that without current-induced field-like SOT field. Our results extend the approaches to determine the SOT switching in the heterostructures with IMA, and will contribute to the research about SOT-based memory and computation.

Acknowledgements

Project supported by the National Natural Science Foundation of China (Grant Nos. 11904017, 11974145, 51901008, and 12004024), Shandong Provincial Natural Science Foundation, China (Grant No. ZR2020ZD28), platform from Qingdao Science and Technology Commission, and the Fundamental Research Funds for the Central Universities of China.

References

[1] Slaughter J M, Rizzo N D, Janesky J, Whig R, Mancoff F B, Houssameddine D, Sun J J, Aggarwal S, Nagel K, Deshpande S, Alam S M, Andre T and LoPresti P *in 2012 IEEE Int. electron devices meeting* 29.23.21

[2] Fukami S, Yamanouchi M, Ikeda S and Ohno H 2014 *IEEE Transactions on Magnetics* **50** 1

[3] Lin X, Yang W, Wang K L and Zhao W 2019 *Nat. Electron.* **2** 274

[4] Liu L, Pai C F, Li Y, Tseng H W, Ralph D C and Buhrman R A 2012 *Science* **336** 4

[5] Liu L, Lee O J, Gudmundsen T J, Ralph D C and Buhrman R A 2012 *Phys. Rev. Lett.* **109** 096602

[6] Miron I M, Garello K, Gaudin G, Zermatten P J, Costache M V, Auffret S, Bandiera S, Rodmacq B, Schuhl A and Gambardella P 2011 *Nature* **476** 189

[7] Pai C, Liu L, Li Y, Tseng H W, Ralph D C and Buhrman R A 2012 *Appl. Phys. Lett.* **101** 122404

[8] Wang M, Cai W, Zhu D, Wang Z, Kan J, Zhao Z, Cao K, Wang Z, Zhang Y, Zhang T, Park C, Wang J, Fert A and Zhao W 2018 *Nat. Electron.* **1** 582

[9] Wang M, Cai W, Cao K, Zhou J, Wrona J, Peng S, Yang H, Wei J, Kang W, Zhang Y, Langer J, Ocker B, Fert A and Zhao W 2018 *Nat. Commun.* **9** 671

[10] Peng S, Zhu D, Li W, Wu H, Grutter A J, Gilbert D A, Lu J, Xiong D, Cai W, Shafer P, Wang K L and Zhao W 2020 *Nat. Electron.* **3** 757

[11] Liu N, Wang H and Zhu T 2012 *Acta Phys. Sin.* **61** 167504 (in Chinese)

[12] Avci C O, Garello K, Gabureac M, Ghosh A, Fuhrer A, Alvarado S F and Gambardella P 2014 *Phys. Rev. B* **90** 224427

[13] Garello K, Miron I M, Avci C O, Freimuth F, Mokrousov Y, Blugel S, Auffret S, Boulle O, Gaudin G and Gambardella P 2013 *Nat. Nanotech.* **8** 587

[14] HayashI M, Kim J, Yamanouchi M and Ohno H 2014 *Phys. Rev. B* **89** 144425

[15] Liu L, Moriyama T, Ralph D C and Buhrman R A 2011 *Phys. Rev. Lett.* **106** 036601

[16] Woo S, Mann M, Tan A J, Caretta L and Beach G S D 2014 *Appl. Phys. Lett.* **105** 212404

[17] Yang H, Zhang B, Zhang X, Yan X, Cai W, Zhao Y, Sun J, Wang K L, Zhu D and Zhao W 2019 *Phys. Rev. Appl.* **12** 034004

[18] Nagaosa N, Sinova J, Onoda S, MacDonald A H and Ong N P 2010 *Rev. Mod. Phys.* **82** 1539

[19] Fukami S, Anekawa T, Zhang C and Ohno H 2016 *Nat. Nanotechnol.* **11** 621

[20] Li Y, Kan H, Miao Y, Yang L, Qiu S, Zhang G, Ren J, Wang C and Hu G 2020 *Chin. Phys. B* **29** 017303

[21] Shi S, Liang S, Zhu Z, Cai K, Pollard S D, Wang Y, Wang J, Wang Q, He P, Yu J, Eda G, Liang G and Yang H 2019 *Nat. Nanotech.* **14** 945

[22] Wang Y, Zhu D, Wu Y, Yang Y, Yu J, Ramaswamy R, Mishra R, Shi S, Elyasi M, Teo K L , Wu Y and Yang H 2017 *Nat. Commun.* **8** 1364

[23] Chen Y T, TakahashI S, Nakayama H, Althammer M, Goennenwein S T B, Saitoh E and Bauer G E W 2013 *Phys. Rev. B* **87** 144411

[24] Liu Y, Chen T, Lo T, Tsai T, Yang S, Chang Y, Wei J and Pai C 2020 *Phys. Rev. Appl.* **13** 044032

[25] Fan X, Wu J, Chen Y, Jerry M J, Zhang H and Xiao J Q 2013 *Nat. Commun.* **4** 1799

[26] Manchon A, Koo H C, Nitta J, Frolov S M and Duine R A 2015 *Nat. Mater.* **14** 871

[27] Ou Y, Pai C, Shi S, Ralph D C and Buhrman R A 2016 *Phys. Rev. B* **94** 140414

[28] Jiang M, Asahara H, Sato S, Ohya S and Tanaka M 2020 *Nat. Electron.* **3** 751

[29] Khvalkovskiy A V, Cros V, Apalkov D, Nikitin V, Krounbi M, Zvezdin K A, Anane A, Grollier J and Fert A 2013 *Phys. Rev. B* **87** 020402

[30] Pai C, Ou Y, Vilela-Leão L H, Ralph D C and Buhrman R A 2015 *Phys. Rev. B* **92** 064426

[31] Katine J A, Albert F J, Buhrman R A, Myers E B and Ralph D C 2000 *Phys. Rev. Lett.* **84** 14

[32] Sun J Z 2000 *Phys. Rev. B* **62** 570

[33] Koch R H, Katine J A and Sun J Z 2004 *Phys. Rev. Lett.* **92** 088302

[34] Nan T, Emori S, Boone C T, Wang X, Oxholm T M, Jones J G, Howe B M, Brown G J and Sun N X 2015 *Phys. Rev. B* **91** 214416

[35] Mazraati H, Zahedinejad M and Åkerman J 2018 *Appl. Phys. Lett.* **113** 092401

[36] Cho S, Baek S C, Lee K D, Jo Y and Park B G 2015 *Sci. Rep.* **5** 14668

[37] Mcguire T R and Potter R I 1975 *IEEE T. Magn.* **11** 1018

[38] Teixeira J M, Silva R F A, Ventura J, Pereira A M, Carpinteiro F, Araújo J P, Sousa J B, Cardoso S, Ferreira R and Freitas P P 2006 *Mater. Sci. Eng. B* **126** 180

[39] Zhu S, Shi G, Zhao P, Meng D, Liang G, Zhai X, Lu Y, Li Y, Chen L and Wu K 2018 *Chin. Phys. B* **27** 076801